AFRL-VS-HA-TR-2004-1035

DESIGN, DEVELOP, TEST AND DELIVER A PROTOFLIGHT MEDIUM-TO-HIGH-ENERGY ELECTRON DETECTOR FOR INTEGRATION INTO A SMALL ON-BOARD DIAGNOSTIC SENSORS PACKAGE

Jeffrey E. Belue
Frederick A. Hanser
Paul R. Morel

Panametrics, Inc.
221 Crescent Street
Waltham, MA 02154-3497

11 March 2004

Final Report

AIR FORCE RESEARCH LABORATORY
Space Vehicles Directorate
29 Randolph Rd
AIR FORCE MATERIEL COMMAND
Hanscom AFB, MA 01731-3010

This technical report has been reviewed and is approved for publication.

/Signed /	/Signed /
KEVIN P. RAY	ROBERT A. MORRIS
Contract Manager	Branch Chief

This document has been reviewed by the ESC Public Affairs Office and has been approved for release to the National Technical Information Service (NTIS).

Qualified requestors may obtain additional copies from the Defense Technical Information Center (DTIC). All others should apply to the NTIS.

If your address has changed, if you with to be removed from the mailing list, or if the addressee is no longer employed by your organization, please notify AFRL/VSIM, 29 Randolph Rd., Hanscom AFB, MA 01731-3010. This will assist us in maintaining a current mailing list.

Do not return copies of this report unless contractual obligations or notices on a specific document require that it be returned.

REPORT DOCUMENTATION PAGE

Form Approved
OMB No. 0704-0188

1. REPORT DATE *(DD-MM-YYYY)*	2. REPORT TYPE	3. DATES COVERED *(From - To)*
11/03/2004	FINAL REPORT	01/09/1995 to 31/01/2004

4. TITLE AND SUBTITLE

Design, Develop, Test and Deliver a Protoflight Medium-to-High-Energy Electron Detector for Integration into a Small On-Board Diagnostic Sensors Package

5a. CONTRACT NUMBER
F19628-95-C-0196

5b. GRANT NUMBER

5c. PROGRAM ELEMENT NUMBER
63410F

6. AUTHOR(S)
Jeffrey E. Belue, Frederick A. Hanser, Paul R. Morel

5d. PROJECT NUMBER
2822

5e. TASK NUMBER
GC

5f. WORK UNIT NUMBER
PM

7. PERFORMING ORGANIZATION NAME(S) AND ADDRESS(ES)

Panametrics, Inc.
221 Crescent Street
Waltham, MA 02154-3497

8. PERFORMING ORGANIZATION REPORT NUMBER

9. SPONSORING/MONITORING AGENCY NAME(S) AND ADDRESS(ES)

Phillips Laboratory
29 Randolf Road
Hanscom AFB, MA 01731-3010
Contract Manager: Kevin Ray AFRL/VSBXR

10. SPONSOR/MONITOR'S ACRONYM(S)

11. SPONSOR/MONITOR'S REPORT NUMBER(S)
AFRL-VS-HA-TR-2004-1035

12. DISTRIBUTION/AVAILABILITY STATEMENT
Approved for public release; distribution unlimited.

13. SUPPLEMENTARY NOTES

14. ABSTRACT

An electron spectrometer has been designed to measure electron flux in the range of 3 to 30 MeV. A breadboard unit was designed and tested, using a solid state detector telescope for geometric factor definition and a Cerenkov radiator/PMT for energy measurement. The measured response to electrons was very broad, so the Cerenkov radiator was redesigned as a larger volume with larger PMTs to improve the energy resolution. The modified Cerenkov radiator/PMT assembly was tested, and a protoflight unit is being fabricated. The protoflight electron spectrometer was originally scheduled to be integrated to the Small Onboard Environmental Diagnostic Sensors (SOBEDS) Package, but this has been canceled. The protoflight is mostly complete, except for the spacecraft electrical interface design, which was on hold until a spacecraft interface was specified. The protoflight sensor is in a configuration where it can be modified for a future flight, using any likely spacecraft interface.

15. SUBJECT TERMS
Electron detector; Cerenkov detector; Electron spectrometer; Electron flux; Proton flux; Space radiation

16. SECURITY CLASSIFICATION OF:			17. LIMITATION OF ABSTRACT	18. NUMBER OF PAGES	19a. NAME OF RESPONSIBLE PERSON
a. REPORT	b. ABSTRACT	c. THIS PAGE			Kevin Ray
Unclassified	Unclassified	Unclassified		26	19b. TELEPHONE NUMBER *(Include area code)* (617) 377-3828

CONTENTS

Figures

Tables

1. INTRODUCTION

High energy electron flux is a very important radiation hazard to spacecraft electronics. Measurement of electron flux along with its variation in time and position across the magnetosphere allows a quantitative understanding of the radiation hazard. The goal of the work described in this report was to design a sensor that measures the high energy electron flux.

A satellite sensor to detect 3 to 30 MeV electrons has been designed and developed. The sensor uses three solid state detectors (SSD) and a quartz Cerenkov radiator. Two SSDs in a telescope configuration form a 9° FWHM detection cone, while the Cerenkov radiator performs the particle energy measurement. The third SSD is behind the Cerenkov radiator, and discriminates electrons from relativistic protons. A fast triple coincidence of the two telescope SSDs and the Cerenkov detector initiates particle analysis. A microcontroller analyzes the detector outputs and stores the counts in a seven-channel electron energy spectrum. Shielding is designed to reduce background count rates in the detectors to minimize random triple coincidences. The design is applicable to spacecraft in the Earth's trapped radiation belts, with the electronics design being hard to >100 kRad.

An initial breadboard sensor, then a modified breadboard sensor were designed, fabricated, calibrated, and tested. A protoflight sensor has been designed, and much of it fabricated. The electrical interface design is not complete, because a spacecraft interface has not been specified. The protoflight spectrometer outline drawing is shown in Figure 1.

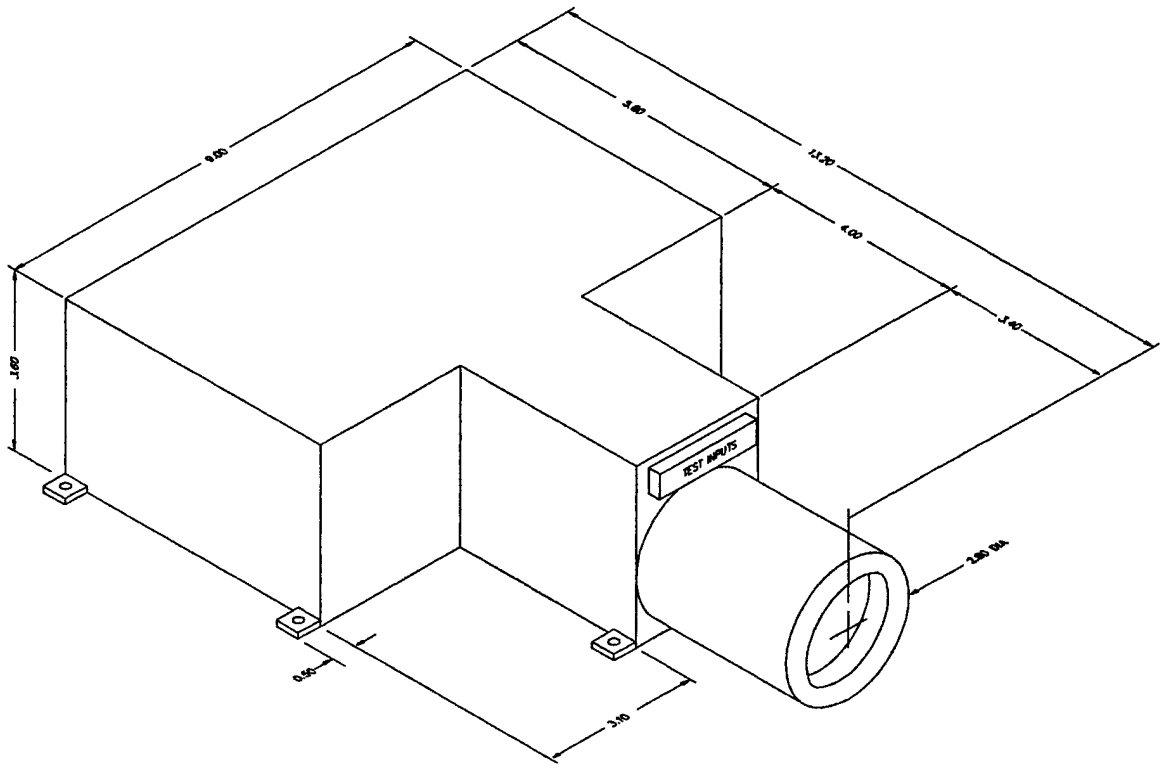

Figure 1 Protoflight Spectrometer Outline Drawing (all dimensions in inches).

The initial breadboard unit was calibrated with protons and electrons. The low-energy proton response is negligible, so non-penetrating protons will not contaminate the electron spectrum. However, the initial breadboard Cerenkov radiator design had a very broad energy response for electrons, and the design was modified to provide better energy resolution. The initial breadboard design, analysis, and test results are described in detail in Reference 1.

2. SENSOR DESIGN, ANALYSIS, AND TEST RESULTS

2.1 Conceptual Design

The initial detector geometry is shown in Figure 2, with the modified detector geometry shown in Figure 3. Two substantial differences between the initial and modified detector assemblies are that four photomultiplier tubes (PMT) and a larger Cerenkov radiator are used in the modified detector design.

A telescope arrangement of two SSDs (D1 and D2) is used to define the sensor field-of-view (FOV), with a 2.5 inch thick quartz Cerenkov radiator providing electron energy selection. A third SSD (D3), behind the Cerenkov radiator, provides discrimination between electrons and high energy, penetrating protons. D1 and D2 are 700 microns thick, 2 cm^2 area totally depleted Si surface barrier detectors. The separation is 3.75 inches, which produces a geometric factor of 0.044 cm^2-sr with a maximum off-axis detection angle of 9.5°. The front collimator extension is used to reduce the D1 geometric factor for lower energy electrons and thus, avoid excessive count rates. A 46 mil Be foil is used to shield D1 from electrons below 0.5 MeV in the FOV. The Cerenkov radiator is 2.5 inches thick quartz, which is the range thickness for 31.76 MeV electrons and 125.5 MeV protons. The Cerenkov radiator has a 1.5 inch square entrance face and a 2.0 inch square rear face. The four sides are flat from front-to-rear, and the design is such that all particles in the D1/D2 telescope FOV must pass completely through the radiator. Two PMTs are mounted side-by-side facing the other two PMTs mounted side-by-side. The remaining area of the radiator is covered with white reflective paint. D3 is a 500 micron partially depleted, 20 cm^2 area Si detector, which covers the entire D1/D2 telescope FOV.

The calculated ionization energy loss in the SSDs and the Cerenkov radiator is shown in Figure 4, while the calculated Cerenkov light produced is shown in Figure 5. These calculations are used to provide the threshold values needed to produce the desired electron energy channels. D1 and D2 have nearly identical responses to electrons (>1 MeV) and protons (>350 MeV) which produce Cerenkov light in the quartz radiator, since the particles are all near the minimum ionization energy loss of 1.5 - 2 MeV-cm^2/g in Si. This is shown in Figure 4, which shows the energy loss for electrons and protons in the three SSDs and in the Cerenkov radiator. The energy losses are calculated from the electron tables of References 2 and 3, and the proton tables of References 4 and 5. Note that the particle energy loss in the Cerenkov radiator should not produce any light, since pure quartz (fused silica) has an extremely low scintillation efficiency.

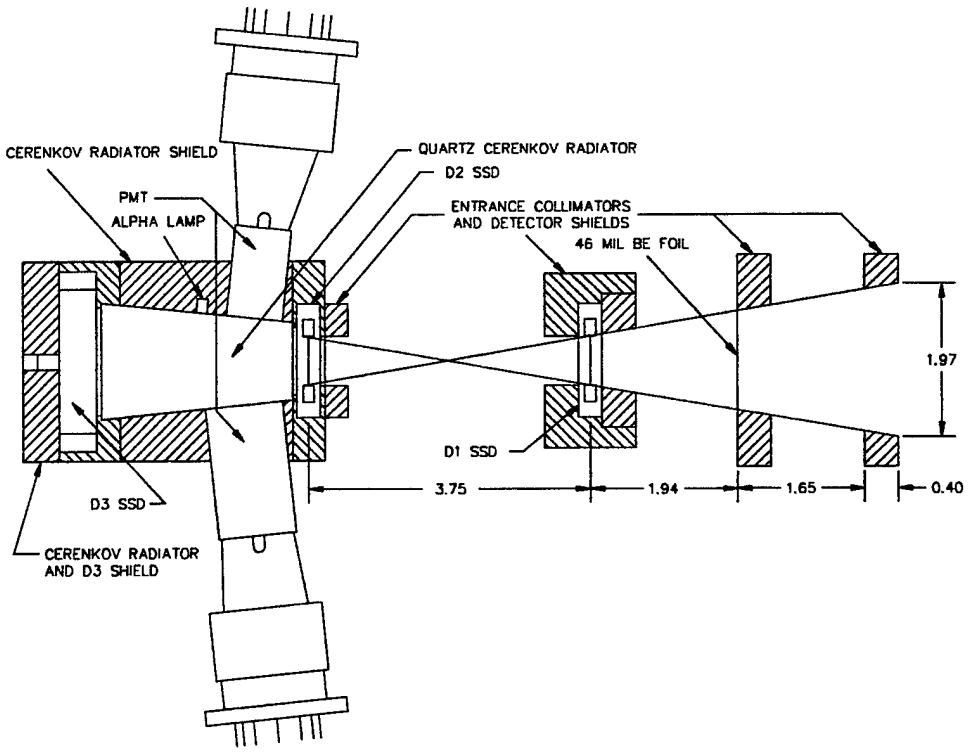

Figure 2 Initial Detector Geometry (all dimensions in inches).

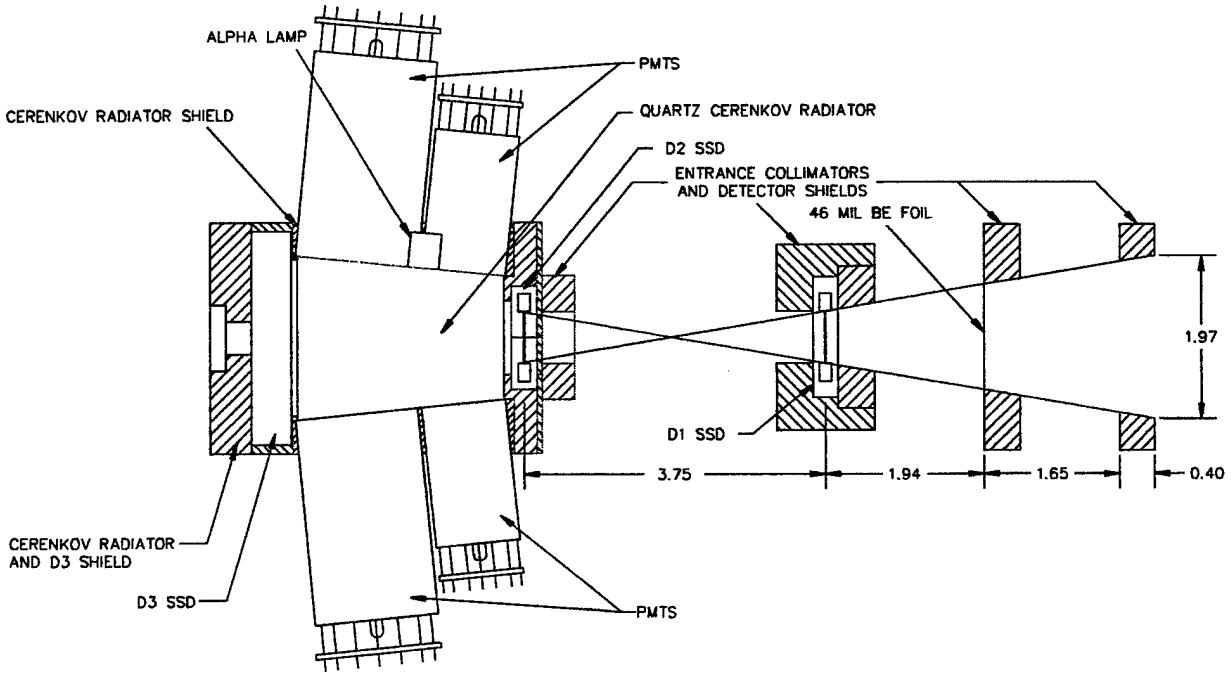

Figure 3 Modified Detector Geometry (all dimensions in inches).

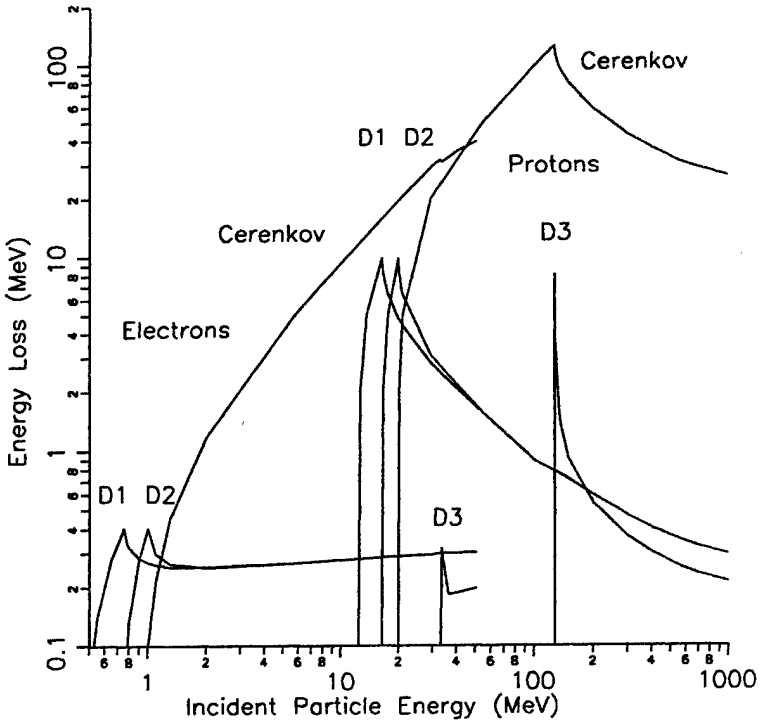

Figure 4 Ionization Energy Loss in the Detectors.

Particle energy discrimination comes from the Cerenkov light output of the radiator, with electron/proton selection coming from D3. The Cerenkov light produced in quartz is (Ref. 6)

$$d^2N/(dxdv) = K\,(1 - 1/(n\beta)^2)\ \text{photons/(cm-(cycles/s))} \tag{1}$$

where N = # of photons, ν = frequency (Hz), x = path length in radiator (cm) and

$$K = 2\pi z^2/(137c) \tag{2}$$

with z the particle charge (in electron charges), v the particle velocity (cm/s), $\beta = v/c$, $c = 3\times10^{10}$ cm/s is the speed of light, and n is the index of refraction (= 1.49 for quartz). For a particle of kinetic energy E and rest mass $E_o = mc^2$,

$$\beta^2 = (E^2 + 2EE_o)/(E + E_o)^2 \tag{3}$$

while the inverse is

$$E = E_o(1/(1 - \beta^2)^{1/2} - 1) \tag{4}$$

The minimum energy for Cerenkov light production is for $\beta_m = 1/n$, so for quartz the electron Cerenkov light threshold ($m_ec^2 = 0.511$ MeV) is 0.178 MeV, and for protons ($m_pc^2 = 938.3$ MeV) it is 327.4 MeV. The stopping power of quartz (S(E) in MeV-cm^2/g) is given for protons in Reference 4, while for electrons it must be calculated from the Si stopping power in Reference 3 and

the O stopping power in Reference 2 using the mass fractions of the elements in quartz (SiO_2). Using the energy loss per cm, $dE/dx = -\rho S(E)$ where $\rho = 2.20$ g/cm^3 is the density of quartz, and converting (1) to wavelength λ by $d\nu = -cd\lambda/\lambda^2$, the PMT photoelectron yield can be written as

$$N_{pe} = \int(QE(\lambda)/\lambda^2)d\lambda \times \int_{E_m}^{E_i} [Kc(1 - 1/(n\beta)^2)/(\rho S(E))]dE \qquad (5)$$

where E_m is the Cerenkov threshold energy and E_i is the energy of the particle when it enters the Cerenkov radiator. $QE(\lambda)$ is the fractional quantum efficiency of the PMT photocathode. The preliminary ruggedized PMT selected has a bialkali photocathode and a borosilicate glass face, giving a response range of 300 to 650 nm with a peak QE of about 0.27 (27 percent), which gives $\int(QE(\lambda)/\lambda^2)d\lambda = 3520$/cm.

The integration over electron and proton energy in (5) was done numerically, using the appropriate range/energy table, to calculate $N_{pe}(E_i)$ for several values of E_i. Note that N_{pe} from (5) is for complete light collection, and the actual value is expected to be about half of the (5) values. For the geometry of Figure 3 the light collection efficiency can be written approximately as

$$L_{ce} = f_A/[1 - (1 - f_A) \times R] \qquad (6)$$

where $f_A \approx 0.214$ is the ratio of total photocathode area (4 PMTs, nominal area) to the total surface area of the Cerenkov radiator, and R is the reflectivity of the white paint. For $R = 0.95$, $L_{ce} = 0.845$, while for $R = 0.98$ (possible with a very high quality $BaSO_4$ coating), $L_{ce} = 0.932$. Using a reasonable estimate of $L_{ce} = 0.5$, a 2.21 MeV electron (corresponding to a 3 MeV incident electron) should produce a signal of about 21 actual photoelectrons, and this is definitely detectable with good quality PMTs. This corresponds to a proton energy threshold of 369 MeV (371 MeV incident energy), so it is also possible to measure proton energy spectra from 371 MeV to above 1000 MeV.

The E_i values of (5) for particles in the FOV must be adjusted for the energy loss in the two telescope SSDs and in the 46 mil Be foil to give an E_{io} value for the incident particle energy. The results for electrons and protons are shown in Figure 4. Since electrons below 31.76 MeV do not penetrate the Cerenkov radiator, they do not produce a D3 pulse, while all protons producing a Cerenkov signal must produce a D3 signal. Thus, the D3 signal is used to distinguish electrons from protons.

The calculated electron energy losses and Cerenkov light outputs assume a straight line path for the electrons. Because of scattering, the actual electron paths are irregular, and thus some electrons above the 31.76 MeV Cerenkov radiator thickness range will still stop within the radiator. The sensor will thus have some reduced response to higher energy electrons, and may be useable for electrons up to 40 MeV.

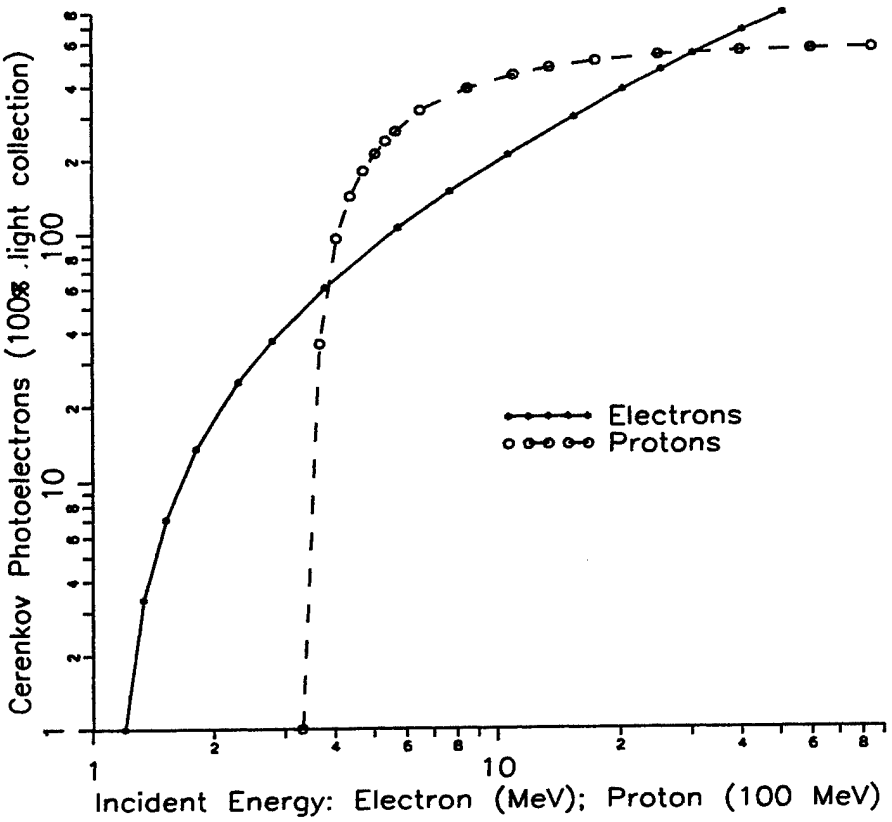

Figure 5 Cerenkov Light Production in the Radiator.

Table 1 SSD Energy Loss Threshold Values				
Detector	Level	Value (MeV)	Particle Energy (MeV)	
			Electrons	Protons
D1	LL	0.13	>0.54	>12.35
"	UL	0.5	-	12.40 - 275
D2	LL	0.13	>0.80	>16.36
"	UL	0.5	-	16.41 - 275
D3	LL	0.13	>33.3	>128

A preliminary set of SSD thresholds is given in Table 1 along with the corresponding incident electron and proton energies. The Cerenkov pulse spectrum is sorted into 8 levels, with the corresponding electron and proton energies being listed in Table 2. The energies in Table 2 are nominal calculations, and in practice will be replaced with calibrated values obtained from actual electron calibration data. Electron (no D3(LL)) and proton (with D3(LL)) spectra are generated by

a fast triple coincidence of D1(LL) * D2(LL) * PMT(LL) ($\tau = 0.1$ μs resolving time), with the energy sorting by PMT(Li). Spectra are only taken for D1 and D2 energy losses in the range of LL to UL, which eliminates possible low-energy proton contamination (protons < 275 MeV). All thresholds are counted, providing several additional counts which allow correction of the measured data for deadtime and random coincidence effects.

Table 2 Cerenkov Light Thresholds and Particle Energies

Cerenkov Level	Calculated Photoelectrons	Particle Energy (MeV)	
		Electrons	Protons
LL	41.6	3.0	371
L1	74.8	4.4	391
L2	149.6	7.8	445
L3	224	11.7	522
L4	299	15.8	626
L5	374	20.	812
L6	449	25.	1179
L7	523	30.	2431

An updated electronics block diagram generated for use with the SOBEDS (Small Onboard Environmental Diagnostic Sensor) Package is shown in Figure 6. The two front SSD (D1 and D2) output signals are amplified and shaped, then the signal is applied to two threshold discriminators (TH/OSs) and a zero cross sensor (Z/C). The PMT output signals are summed, amplified and shaped and then applied to a low level threshold discriminator (TH/OS), a zero cross sensor (Z/C) and an array of seven additional threshold discriminators (TH/OS). The rear SSD (D3) output signal is amplified and shaped, then applied to a single threshold discriminator (TH/OS). A small "alpha lamp" (a small scintillator piece with a weak Am-241 alpha particle emitter embedded in the scintillator) is used to monitor and set the PMT gain, both on the ground and in orbit (during low ambient background periods).

Incident electrons greater than 3.0 MeV within the FOV trigger the D1, D2 and PMT zero cross sensors, yielding a fast coincidence (FAST COINC) output pulse (COINC). Incident protons greater than 371 MeV within the FOV also trigger the D1, D2 and PMT zero cross sensors; however, these particles also trigger the rear SSD (D3) threshold (TH/OS). The COINC pulse latches the state of the SSD and PMT TH/OSs and interrupts the microcontroller, which reads and resets the latches, and increments a random access memory (RAM)-based COINC pulse counter. Based on the state of the latches, the microcontroller also increments one of an array of RAM-based counters. The microcontroller then returns to its background processing task, until it is again interrupted by a COINC pulse. Thus, seven differential-channel and one integral-channel energy analyses of electrons from 3.0 to >30. MeV, and of protons from 371 to >2431 MeV are performed. The SSD and PMT TH/OS and FAST COINC output pulses are also accumulated in hardware counters, which are periodically read and reset by the microcontroller in order to establish a dead-time-correction factor.

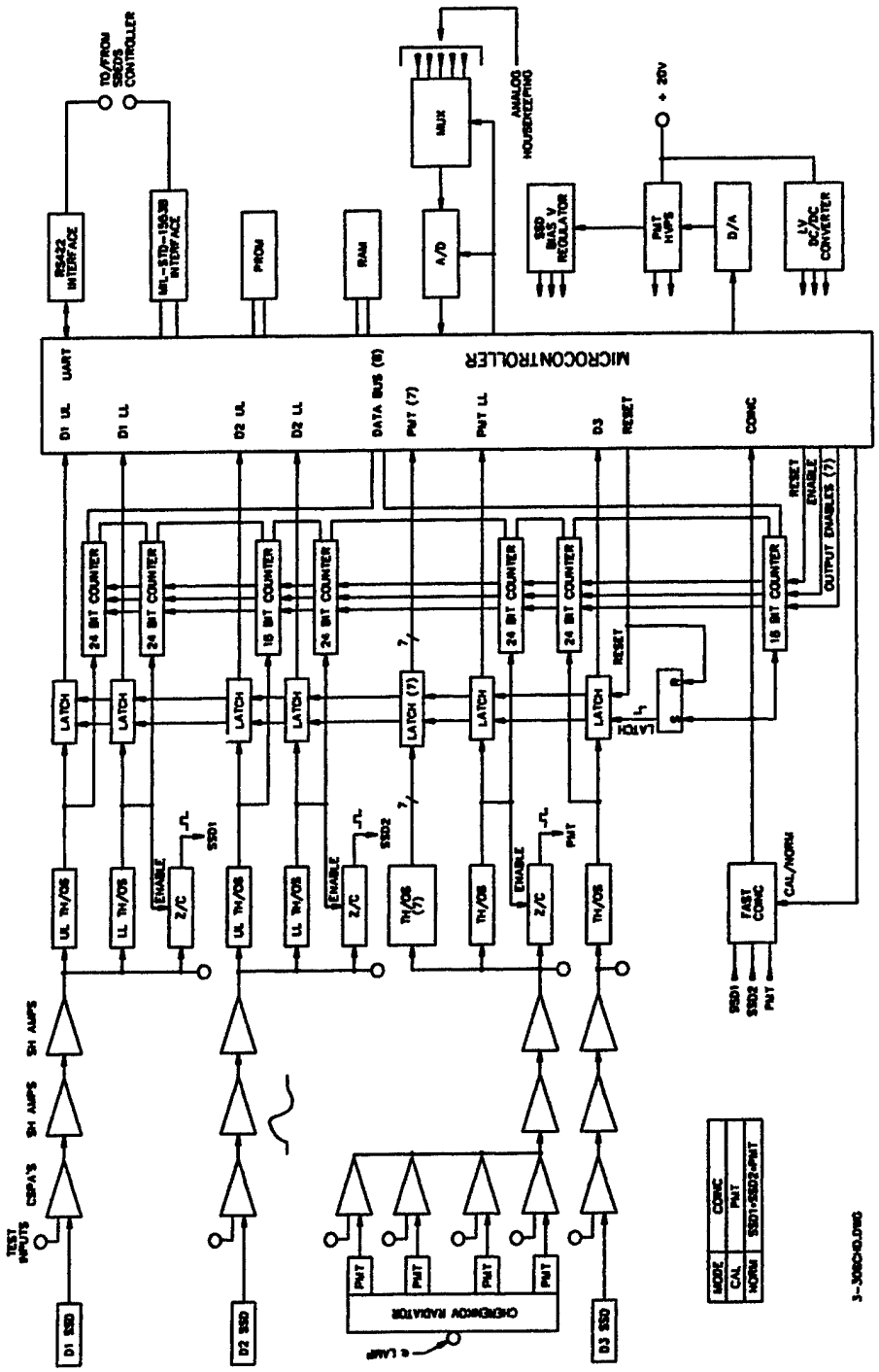

Figure 6 Spectrometer Electronics Block Diagram.

It was anticipated that data packets would be transferred to the SOBEDS Package central processing unit via a buffered universal asynchronous receiver/transmitter (UART). The Spectrometer microcontroller would format the Spectrometer data in a packet structure defined by the SOBEDs interface. During the latter part of 2000 the use of the Spectrometer for SOBEDS was no longer viable, but a possible use on the AFRL/NASA IMEX spacecraft arose. This was explored for several months, but in early 2001 NASA dropped out of the program and it was canceled. There was no flight set for the Spectrometer, so the interface electronics design was kept on hold. This was a cost effective approach, since it avoids fabricating an interface PCB which would have to be redesigned and a new one fabricated after a specific spacecraft interface was provided.

2.2 Modified Breadboard Detector

The measured electron responses of the initial Cerenkov detector show that the response is more a set of integral electron channels, rather than differential channels. This is partly the result of using only two PMTs, also partly the result of a small Cerenkov radiator, where some high energy electrons scatter (leak) out of the sides and thus generate only a fraction of the full Cerenkov light for an electron that stops in the radiator. The desired response to high-energy electrons is for differential channels, since the deconvolving of integral channel responses is less accurate. Thus, the initial detector assembly design was modified then retested. The modified breadboard detector assembly is housed in the same steel NEMA electrical enclosure that was used for the initial design, as shown in Figure 7. The modified breadboard Cerenkov radiator is larger than the initial radiator, as is shown in Figure 8. The modified design allows for larger PMTs mounted to the radiator sides. Also, there are four PMT's (PMT1=1", PMT2=1", PMT3=1.5" and PMT4=1.5" diameter photocathodes) in place of the initial detector array using only two PMT's (PMT1=0.75" and PMT2=1" diameter photocathodes).

The Cerenkov radiator has a reflective paint ($BaSO_4$) on all surfaces except PMT mounting surfaces and the alpha lamp mounting surface. In addition, a thin layer of aluminum foil is mounted on the outside of the paint. The modified design improves the light collection efficiency of the detector array to satisfy the energy resolution goals of this instrument.

Testing was done at Panametrics using radioactive sources, atmospheric muons and electrons at Rensselaer Polytechnic Institute (RPI) Linear Accelerator, in Troy NY.

2.3 Analog Signal Processing Electronics

The signal processing electronics consists of the D1, D2, charge-sensitive preamplifiers (CSPA), PMT buffer amplifiers, PMT summing amplifiers, shaping amplifiers (SH AMP), threshold discriminators/one shots (TH/OS) and zero-cross sensors (Z/C).

Each of the functional blocks, titled TH/OS in Figure 6, consists of an analog threshold (TH) discriminator whose output is input to a timing element called a one shot (OS). The OS provides critical timing that is generally designed with discrete hardware (monostable multivibrator) for each TH/OS functional block. A single Field Programmable Gate Array (FPGA) has been designed and tested to implement the OS function, digitally. Since seven different analog signal paths require the OS function, the FPGA use saves a significant amount of Printed Circuit Board (PCB) space. Reducing PCB space helps to keep the overall spectrometer package size small, and reduces instrument mass. Fast coincidence logic was also designed into the same FPGA.

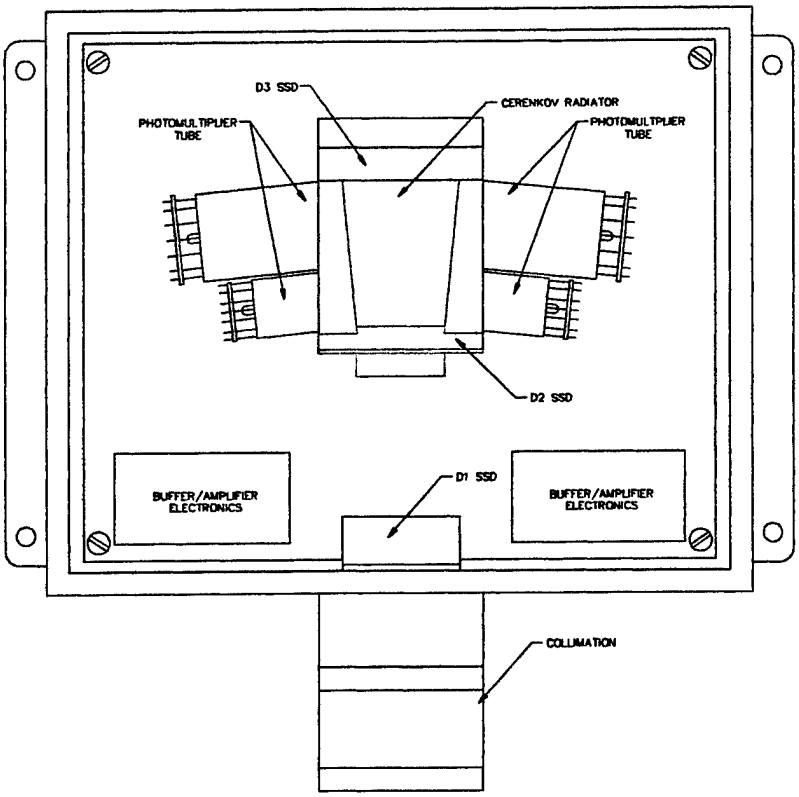

Figure 7 Breadboard Detector Assembly.

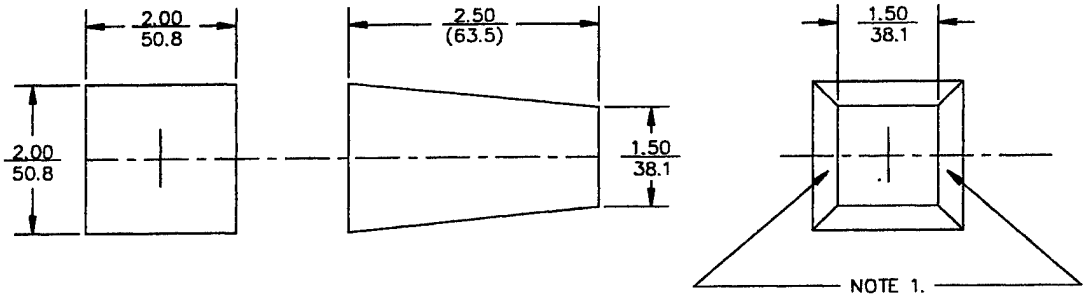

NOTES:
1. THESE 2 POLISHED SURFACES: { SURFACE QUALITY; 60/40 (SCRATCH/DIG), FLATNESS; 1 WAVELENGTH PER INCH

   ALL OTHER SURFACES, AS MACHINED.
2. TOL. ±.01 (0.254)
3. MATERIAL: FUSED SILICA, CORNING 7940 INCLUSION CLASS 0, HOMOGENEITY GRADE F OR EQUIVALENT.

CERENKOV RADIATOR
FRUSTUM OF PYRAMID WITH FOUR SIDES SK-7147B

Figure 8 Modified Cerenkov Radiator Design.

2.4 Digital Electronics

The digital electronics consists of latches and counters that interface to the analog discriminators and the microcontroller (μC) with its associated support, including the spacecraft interface. The baseline design uses an industry standard microcontroller architecture, Intel's 8XC51FC, manufactured by United Technologies Microelectronics Center (UTMC), UT69RH051, which is radiation hard to a total dose of 1×10^6 rad and is latch-up immune. Microcontroller internal features include:

* Three programmable 16-bit timer/counters
* Internal clock/oscillator, of static design, controlled by an external crystal
* 256 bytes of on-chip [internal] Read/Write Memory
* Industry standard MCS®-51 instruction set
* 64k of external program and data memory space
* Universal asynchronous receiver/transmitter (UART)

The microcontroller executes its program from external rad-hard non-volatile PROM. Since the μC operates out of PROM, unambiguous program operation is guaranteed. The proposed design does not allow for on-orbit changes to the program; however, the design can easily be changed to accommodate this should it be needed. The initial design uses external Read/Write Memory (RAM) to augment the microcontroller's internal memory. During the final design phase we will examine the memory requirements, in detail, to eliminate external volatile memory if possible.

A watchdog timer provides a measure of CPU fault tolerance by activating the microcontroller's hardware reset if it times out. This provides a means to recover from a Single Event Upset (SEU) event that will induce errors or other anomalous conditions. Part of the flight software housekeeping procedure is to reset the watchdog periodically. If a watchdog timeout occurs, the microcontroller is reset and program operation begins from a known configuration. All watchdog events are reported in the spacecraft digital serial telemetry stream.

The heart of the logic needed for microcontroller support will be implemented with a Field Programmable Gate Array (FPGA). A second FPGA provides detector pulse latching and counting along with peripheral decoding, watchdog timing, spacecraft telemetry timing and various housekeeping functions. Figure 9 shows the functions designed for the Digital Processing FPGA.

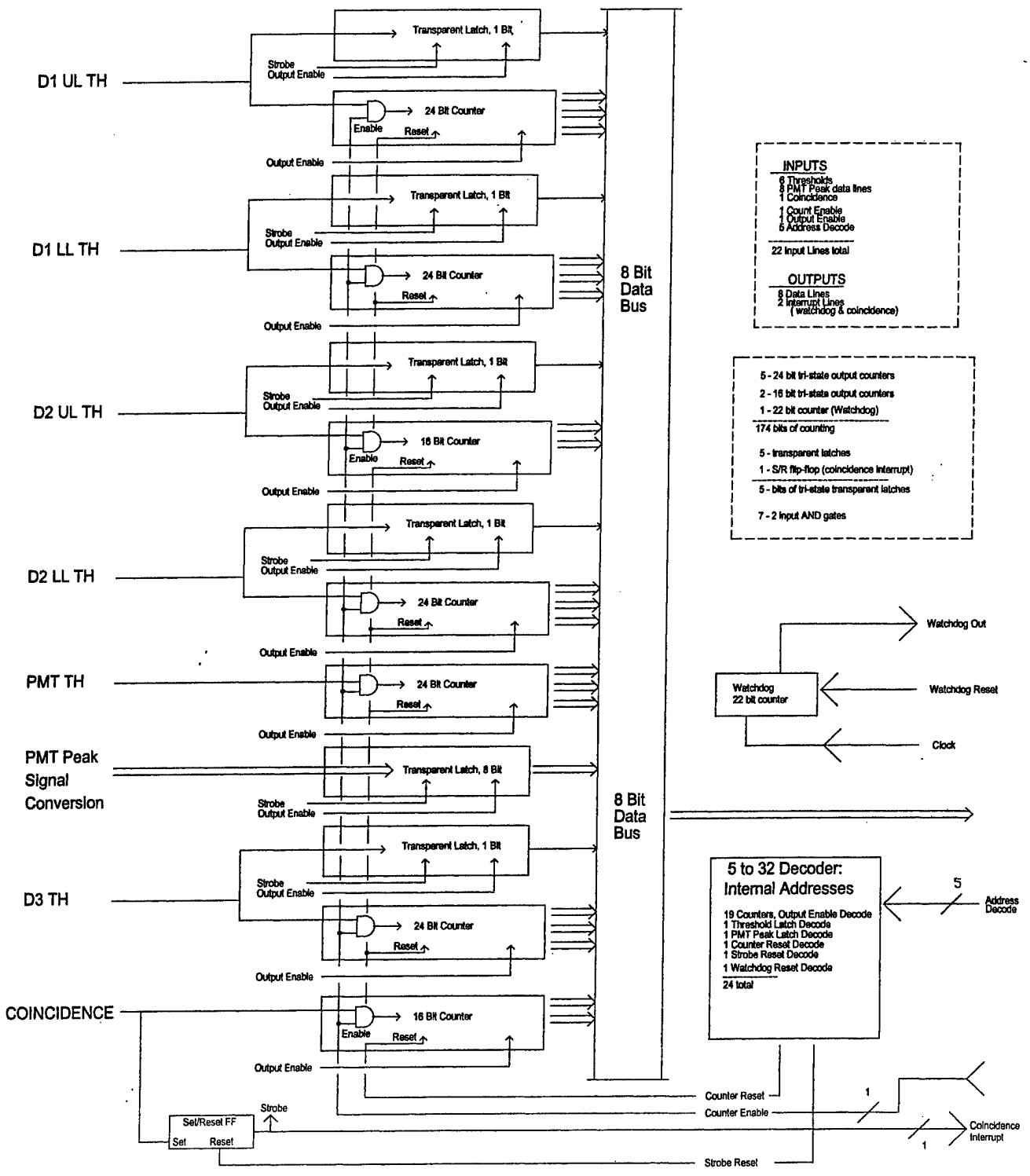

Figure 9 Digital Processing FPGA.

2.5 Modified Breadboard Calibration Data Analysis

A brief summary of the analysis of the modified breadboard calibration data is provided below.

2.5.1 Atmospheric Muon Test Results

Atmospheric muons are a particle source to verify basic operation and provide initial data used to determine PMT response. Figure 10 shows the muon response compared with the response to 8.9 MeV electrons. Note that this provides a cross calibration so that atmospheric muon response can be used to calibrate the alpha lamp peak, and thus set the PMT gain for electron response.

2.5.2 Electron Tests at the RPI Linear Accelerator

The modified breadboard Cerenkov detector was calibrated, at RPI, with electrons in the energy range of 3.0 MeV to 33.3 MeV. The results show sufficient energy resolution for seven differential channels for electrons and protons and one integral channel for electrons (> 30 MeV) and protons (> 2430 MeV). Some of the measured electron responses are shown in Figures 11 and 12.

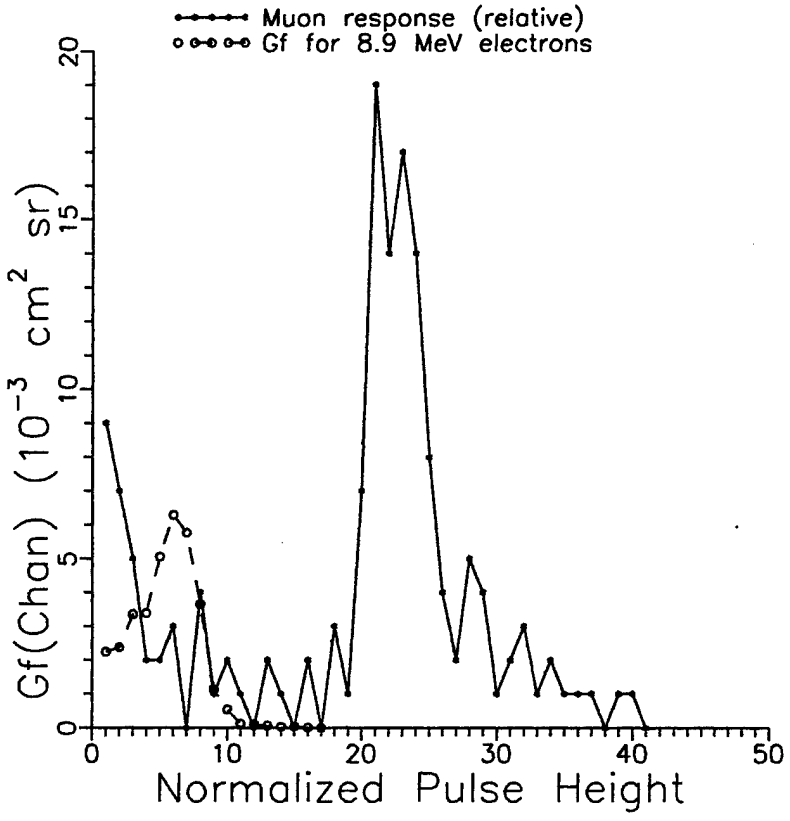

Figure 10 Muon Response and 8.9 MeV Electron Response.

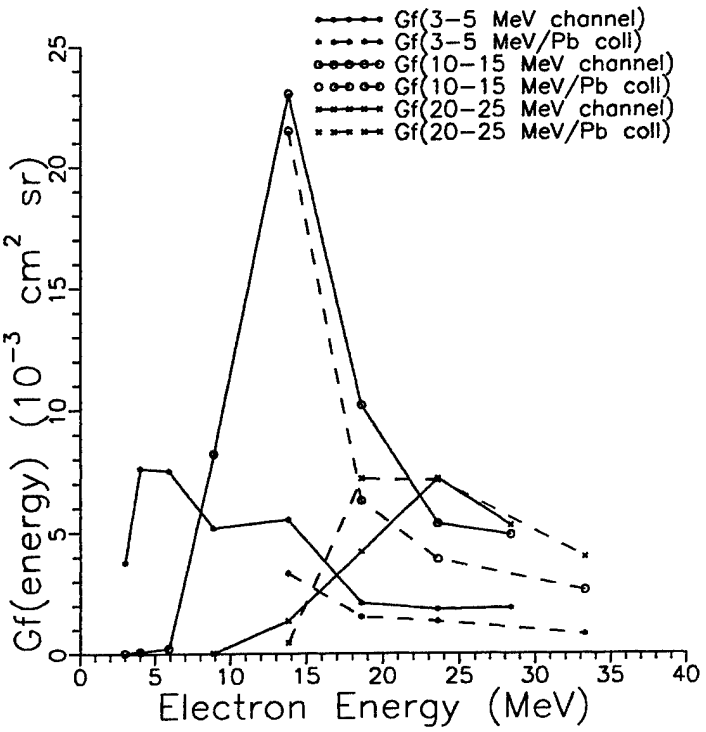

Figure 11 Electron Response vs. Electron Energy for Three Energy Channels.

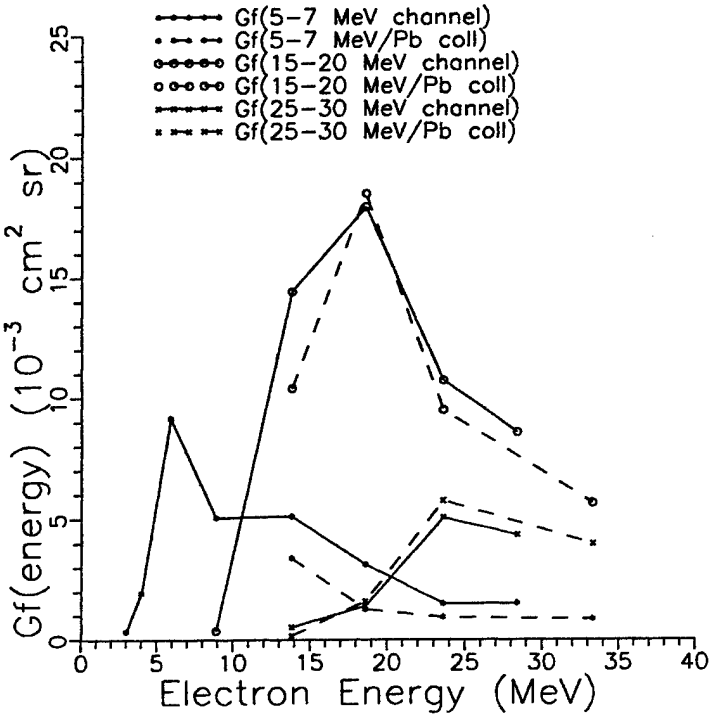

Figure 12 Response vs. Electron Energy for Three Energy Channels.

3. SENSOR DESIGN STATUS

Following the Critical Design Review on 11 September, 1998, the electronics design was completed. However, as noted previously, the interface design is currently on hold, since there is no spacecraft designated for the Spectrometer.

The modified Cerenkov radiator protoflight detector assembly has the following characteristics:

(1) Truncated pyramid-shaped radiator.

(2) Four PMTs; two 1.0 inch and two 1.5 inch.

(3) Three planar SSDs; two 2 cm^2 in the front telescope and one 20 cm^2 behind the radiator.

3.1 Analog Signal Processing

The analog processing breadboard electronics that have been designed and built include Charge Sensitive Preamplifiers (CSPA), buffer amplifiers, a summing amplifier, the shaping amplifiers and all the threshold detectors.

3.2 High Voltage Power Supply

The high voltage power supplies were tested during the spectrometer calibration and operate satisfactorily. Modifications necessary due to the addition of two PMTs have been completed. The PCBs have been designed, fabricated, assembled, and tested.

3.3 Digital Processing

Design of the microcontroller circuitry has been completed. Hardware and software designs are complete to the point that the design of the digital processing FPGA has been completed (Figure 9). The proposed spectrometer telemetry format is shown in Table 3. However, the complete software design depends on the spacecraft interface, so this must wait until a specific spacecraft interface is provided.

3.4 Mass, Power and Summary of Characteristics

Table 4 lists a summary of the spectrometer characteristics including mass and power. Adjustments to the mass reflect the increased shielding needed for the collimators and changes to the Cerenkov radiator. Tungsten (W) and copper (Cu) will replace the aluminum collimators. The power requirements changed only slightly due to the addition of two PMTs.

3.5 Spacecraft Interface

The spacecraft provides a +28V Main Bus for the Spectrometer. Commands and telemetry with the spacecraft are assumed to be similar to that for the APEX spacecraft. The interfacing hardware is expected to be similar to the industry standard RS422 balanced (differential) transmitter/receivers. We plan to examine the MIL-STD-1553 Remote Terminal interface/protocol that will allow an interface to different spacecraft busses. However, as noted previously, the interface

design is not complete since there is no specified spacecraft interface.

4. SENSOR STATUS

The sensor status is as follows:

1) Assembly and testing of the Sensor electronics has been partially completed. The interface PCB design must be completed, and the PCB fabricated and tested, after a spacecraft interface has been defined.

2) Assembly of the detector section is mostly complete. The mechanical housing design must be finalized, fabricated, and assembled.

3) The completed sensor must be calibrated for electronic gains and thresholds. The final completed sensor must be calibrated at the RPI Linear Accelerator to provide the final electron response.

4) The calibrated sensor must undergo protoflight testing - vibration, EMI/EMC testing, and thermal vacuum testing.

5) The AFRL must be supported as necessary for placing the Sensor on the selected spacecraft.

Table 3 Proposed Spectrometer Telemetry Packet			
Data	Number of Bytes	Data	Number of Bytes
SSD1 LL TH/OS Hardware Counter	3	RAM Counter 11 (445 - 522 MeV p)	2
SSD1 UL TH/OS Hardware Counter	3	RAM Counter 12 (522 - 626 MeV p)	2
SSD2 LL TH/OS Hardware Counter	3	RAM Counter 13 (626 - 812 MeV p)	2
SSD2 UL TH/OS Hardware Counter	2	RAM Counter 14 (812 - 1180 MeV p)	2
PMT TH/OS Hardware Counter	3	RAM Counter 15 (1180 - 2430 MeV p)	2
SSD3 TH/OS Hardware Counter	3	RAM Counter 16 (>2430 MeV p)	2
Fast Coincidence Hardware Counter	2	RAM Counter 17 (Diagnostic count)	2
RAM Counter 1 (3.0 - 4.4 MeV el)	2	RAM Counter 18 (Diagnostic count)	2
RAM Counter 2 (4.4 - 7.8 MeV el)	2	RAM Counter 19 (Diagnostic count)	2
RAM Counter 3 (7.8 - 11.7 MeV el)	2	RAM Counter 20 (Diagnostic count)	2
RAM Counter 4 (11.7 - 15.8 MeV el)	2	RAM Counter 21 (Diagnostic count)	2
RAM Counter 5 (15.8 - 20 MeV el)	2	RAM Counter 22 (Diagnostic count)	2
RAM Counter 6 (20 - 25 MeV el)	2	RAM Counter 23 (Triple Coincidences)	2
RAM Counter 7 (25 - 30 MeV el)	2	Analog Subcommutator	1
RAM Counter 8 (>30 MeV el)	2	Bilevel Subcommutator	1
RAM Counter 9 (371 - 391 MeV p)	2	Cal/Norm Flag and Subcomm Frame Identifier	1
RAM Counter 10 (391 - 445 MeV p)	2	Checksum	2
70 Bytes Total			

Table 4 Spectrometer Summary of Characteristics	
Detectors	3 planar silicon solid state detectors and a Cerenkov radiator with two photo multipliers in a telescope configuration
Field-of-View	9.5° maximum Field-of-View (FOV) angle
Energy Ranges	Electrons: 3 MeV to >30 MeV Protons: 371 MeV to >2430 MeV
Output Data Format	560 bits (70 bytes) serial, read once per second, includes commutated analog monitors
Command Requirements	possible: Normal Mode, Calibration Mode, HVPS level (1 of 8), Data Request
Size	11.40 L X 9.00 W X 3.60 H (inches)
Mass	~10 lbs (4.5 kg)
Power	~1.0 W
Temperature Range	0° C to +30° C Nominal Operating -20° C to +35° C Maximum Operating -20° C to +40° C Non Operating
Geometric Factors, Proton	0.044 cm^2 sr
Geometric Factors, Electron	0.01 cm^2 sr at ~3 MeV ; 0.03 cm^2 sr for > 10 MeV

REFERENCES

1. J. E. Belue, F. A. Hanser and P. R. Morel (16 June 1997), *Design, Develop, Fabricate, Test and Deliver a Protoflight Medium-to-High-Energy Electron Detector for Integration into a Small On-board Diagnostic Sensors Package*, PL-TR-97-2082, ADA328471.

2. M. J. Berger and S. M. Seltzer (1964), Tables of Energy Losses and Ranges of Electrons and Positrons, NASA SP-3012.

3. M.J.Berger and S.M.Seltzer (1966), *Additional Stopping Power and Range Tables for Protons, Mesons, and Electrons*, NASA SP-3036.

4. J.F.Janni (1982), "Proton Range-Energy Tables, 1 keV - 10 GeV; Part 1. Compounds," *Atomic Data and Nuclear Data Tables*, **27**, No. 2/3, 147-339 (March/May).

5. J.F.Janni (1982), "Proton Range-Energy Tables, 1 keV - 10 GeV; Part 2. Elements," *Atomic Data and Nuclear Data Tables*, **27**, No. 4/5, 341-529 (July/September).

6. A.H.Snell (1962), editor, "Nuclear Instruments and Their Uses," **Vol. 1**, Wiley, NY.